

# CrystEngComm

Accepted Manuscript



This is an *Accepted Manuscript*, which has been through the Royal Society of Chemistry peer review process and has been accepted for publication.

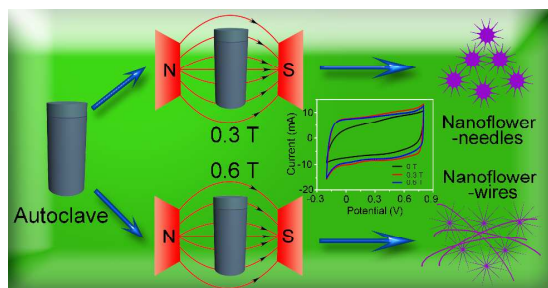
*Accepted Manuscripts* are published online shortly after acceptance, before technical editing, formatting and proof reading. Using this free service, authors can make their results available to the community, in citable form, before we publish the edited article. We will replace this *Accepted Manuscript* with the edited and formatted *Advance Article* as soon as it is available.

You can find more information about *Accepted Manuscripts* in the [Information for Authors](#).

Please note that technical editing may introduce minor changes to the text and/or graphics, which may alter content. The journal's standard [Terms & Conditions](#) and the [Ethical guidelines](#) still apply. In no event shall the Royal Society of Chemistry be held responsible for any errors or omissions in this *Accepted Manuscript* or any consequences arising from the use of any information it contains.

## The table of contents entry

An electrode of the  $\text{MnO}_2$  nanostructures with  $2 \times 2$  tunnels prepared via magnetic-field-assisted hydrothermal synthesis exhibited an enhanced specific capacitance (306 F/g) and excellent cyclic stability.



Cite this: DOI: 10.1039/c0xx00000x

www.rsc.org/xxxxxx

ARTICLE TYPE

# Magnetic-field-assisted hydrothermal synthesis of 2 × 2 tunnels of MnO<sub>2</sub> nanostructures with enhanced supercapacitor performance

Jiajia Shao,<sup>a, ‡</sup> Wenyao Li,<sup>a,b, ‡</sup> Xiying Zhou<sup>a,\*</sup> and Junqing Hu<sup>b,\*</sup>

Received (in XXX, XXX) Xth XXXXXXXXXX 200X, Accepted Xth XXXXXXXXXX 200X

DOI: 10.1039/b000000x

An effective magnetic-field-assisted hydrothermal synthesis was used to induce the growth of 2×2 tunnels MnO<sub>2</sub> nanostructures for the supercapacitor application. As-fabricated electrode from the MnO<sub>2</sub> nanostructures exhibited an enhanced specific capacitance of 306 F/g at 0.5 A/g and desirable cyclic stability, which considerably exceeds the performance of MnO<sub>2</sub> material prepared without and with high magnetic field, making them a promising electrode material for supercapacitors.

## 1. Introduction

Electrochemical capacitors, also called supercapacitors, store energy using either ion adsorption (electrochemical double layer capacitors) or fast surface redox reactions (pseudocapacitors)<sup>[1]</sup>. Especially, the pseudocapacitors have attracted intense interests recently due to the merits of high specific capacitance, long lifecycle and high power density<sup>[2]</sup>. The main used active electrode materials can be classified into carbon, conducting polymers and transition metal oxides<sup>[3-6]</sup>. Regarding these materials, MnO<sub>2</sub> has stood out as the most promising material owing to its high theoretical specific capacitance, low-cost, abundance and environmentally friendly nature<sup>[7-9]</sup>. Among crystal structures ( $\alpha$ ,  $\beta$ ,  $\gamma$ , and  $\delta$  type) of MnO<sub>2</sub> material,  $\alpha$ -MnO<sub>2</sub> is widely used as the electrode material because of its 2 × 2 tunnels that favors the storage of electrolytic cations in view of their large size thereby increasing diffusion and capacitance<sup>[10]</sup>.

As we all know, magnetic field, similar to the conventional reaction conditions such as pressure and temperature, has been introduced as an effective tool to control chemical reactions and material synthesis owing to its influence on the electrical conductivity, crystal structure and morphology of various materials<sup>[11-17]</sup>. For instance, Hone *et al*<sup>[11]</sup>, have demonstrated the electric conductivity of the carbon nanotubes is 24 times higher in the parallel direction than that in the perpendicular due to the effect of magnetic field. Additionally, hydrothermal synthesis is a facile technique to prepare MnO<sub>2</sub> electrode materials by choosing the reaction temperature or time properly<sup>[18-20]</sup>. But till now, there is no study on combining the advantages of the magnetic field and hydrothermal route to synthesize electrode materials with the aim of enhancing the electrochemical performance, though the individual property of both has been extensively investigated. In this way, we try to prepare MnO<sub>2</sub> nanostructures as an electrode material for supercapacitor with competitive advantages such as

rich accessible electroactive sites, rational crystal structure and lower charge transfer resistance.

Herein, we report an effective magnetic-field-assisted hydrothermal synthesis to induce the growth of MnO<sub>2</sub> nanostructures. With the magnetic strength increasing, the crystal structure of MnO<sub>2</sub> changes from tetragonal phase of  $\alpha$ -MnO<sub>2</sub> to orthorhombic phase of  $\gamma$ -MnO<sub>2</sub>; importantly, as-fabricated electrode from the MnO<sub>2</sub> nanostructures exhibited an enhanced specific capacitance of 306 F/g at 0.5 A/g, which considerably exceeds the value of MnO<sub>2</sub> material prepared without and with high magnetic field. In addition, the specific capacitance of  $\alpha$ -MnO<sub>2</sub> electrode demonstrated an excellent cycle stability, i.e., nearly 95.3% retention after 5000 cycles.

## 2. Experimental Section

### 2.1 Preparation

Analytical grade 0.05 g of PVP and 40 mL 0.02 M KMnO<sub>4</sub> aqueous solution were mixed with vigorously magnetic stirring and then transferred into a Teflon-lined stainless steel autoclave (50 mL capacity), which was fixed between two permanent magnets poles. The strength of the magnetic fields was 0, 0.3 and 0.6 T, respectively. After that, the whole reaction cells were put into an oven and kept at 140°C for 12 h, then cooled down to room temperature naturally. The products were filtered and washed several times with distilled water and absolute ethanol, and finally dried in vacuum oven at 60°C for 12 h. All the other parameters were fixed as the strength of the magnetic field changed.

### 2.2 Material Characterizations

The X-ray powder diffraction analysis was performed on a Rigaku D/max-2500 PC X-ray diffractometer (Cu-K $\alpha$  radiation). The morphologies of the products were studied by field emission scanning electron microscope (SEM; S-4800) equipped with an energy dispersive X-ray spectrometer (EDS), and transmission electron microscope (TEM; JEM-2010F). Their magnetic properties were evaluated on a LakeShore-7407 vibrating sample magnetometer (VSM), and the field reached up to 1.8 T. The mass of the electrode materials was weighed on an XS analytical balance (Mettler Toledo;  $\delta=0.01$  mg).

### 2.3 Electrochemical Characterizations

Electrochemical performances of the as-obtained products were performed on an Autolab (PGSTAT302N potentiostat)

using a three-electrode mode in a 0.5 M Na<sub>2</sub>SO<sub>4</sub> solution. Working electrodes were prepared by mixing the as-synthesized MnO<sub>2</sub> products (80 wt%) with acetylene black (15 wt%), and poly(tetrafluoroethylene) (5 wt%). A small amount of N-methylpyrrolidinone was then added to the mixture. The mixture was then dropped onto graphite paper and dried at 80 °C overnight to remove the solvent. The reference electrode and counter electrode were saturated calomel electrode (SCE) and platinum (Pt) foil, respectively. Standard current-voltage (C-V) curves were measured between -0.2 and 0.8 V. The specific capacitance [F g<sup>-1</sup>] and current density [A g<sup>-1</sup>] were calculated based on the mass of active materials. The mass of MnO<sub>2</sub> active materials per unit area (~1x1 cm<sup>2</sup>) of the electrode is about ~0.72, 0.62 and 0.68 mg/cm<sup>2</sup> for 0, 0.3 and 0.6 T, respectively.

### 3. Results and Discussion

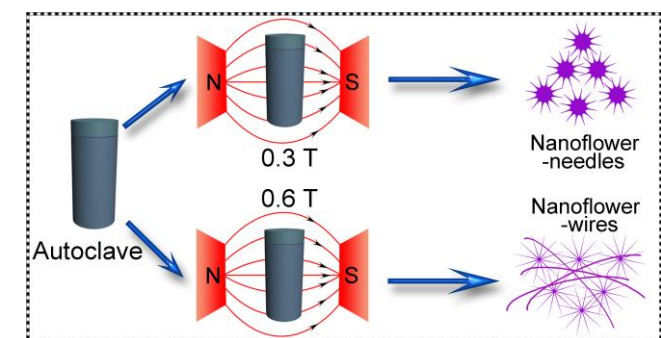


**Fig. 1** Schematic illustration of the formation of the MnO<sub>2</sub> nanostructures in magnetic field.

The MnO<sub>2</sub> nanostructures were facily synthesized through magnetic-field-assisted hydrothermal synthesis. The stainless steel autoclave was fixed between two permanent magnets poles, which was shown in Fig. 1, the strengths of the magnetic fields on the inner surface of the cells were 0.3 and 0.6T, respectively. The evolutions of the MnO<sub>2</sub> morphology are examined by SEM firstly. For the MnO<sub>2</sub> prepared without magnetic field (Fig. 2a, b), a large quantity of uniformly sized nanoflowers are observed (with a mean diameter of ~ 70 nm). When 0.3T magnetic field was applied, the nanoflowers gradually evolved to nanoflower-needle structure (Fig. 2c, d), which many tiny nanoneedles grew from the initially formed nanoflowers with their diameter decreasing to ~ 60 nm. Fig. 2e (also Fig. 2f) shows the MnO<sub>2</sub> nanoflower-wires prepared at 0.6T, except for the continuous decrease of their diameter (~ 40 nm), a large amount of MnO<sub>2</sub> nanowires (with a length longer than 1 μm) evolved from the original nanoneedles are obtained, and consequently the accessible electroactive sites or “active” surfaces are significantly increased. Thus, there was a strong correlation between the applied magnetic field and the morphology of the MnO<sub>2</sub> nanostructure.

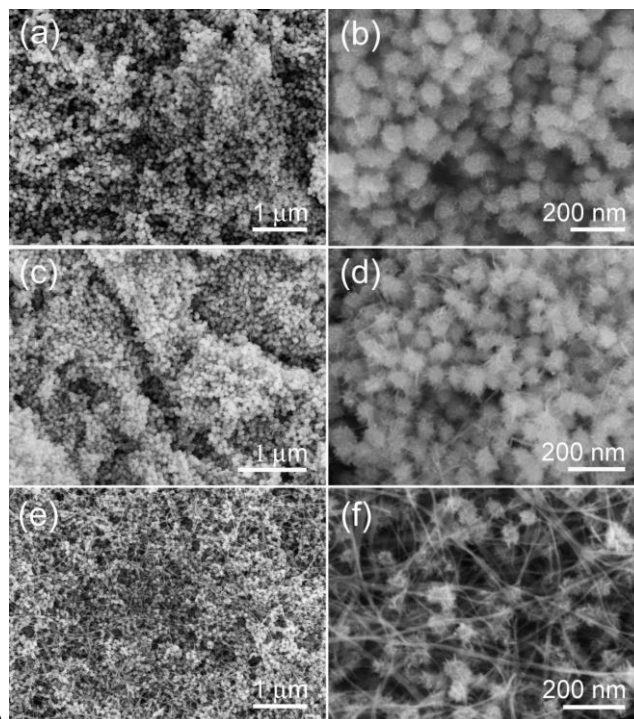


**Fig. 2** (a, b) Low and high magnification SEM images of MnO<sub>2</sub> nanoflowers at 0T, (c, d) MnO<sub>2</sub> nanoflower-needles at 0.3T, (e, f) MnO<sub>2</sub> nanoflower-wires at 0.6T.

The XRD patterns of the product prepared at 0T (Fig. 3a) confirm the presence of α-MnO<sub>2</sub> (JCPDS: 44-0141; I4/m(87)) with 2 × 2 tunnels structure and poor crystallinity. Increasing the magnetic field to 0.3T, the XRD patterns suggests α-MnO<sub>2</sub> with better crystallinity. Specially, there contains an increase in crystallinity and crystalline transformation when the magnetic field increases from 0.3 to 0.6T, as evidenced by the appearance of new sharp reflection peaks (marked by \*), which are indexed to γ-MnO<sub>2</sub> (JCPDS: 44-0142; I4/m(87)) ramsdellite with 1 × 2 tunnels structure. So, increasing the magnetic strength could lead to an evolution from the tetragonal phase (2 × 2 tunnels) to orthorhombic phase (1 × 2 tunnels), schematic representation of the MnO<sub>2</sub> tunnel structures is shown in Fig. 3b and 3c, respectively.

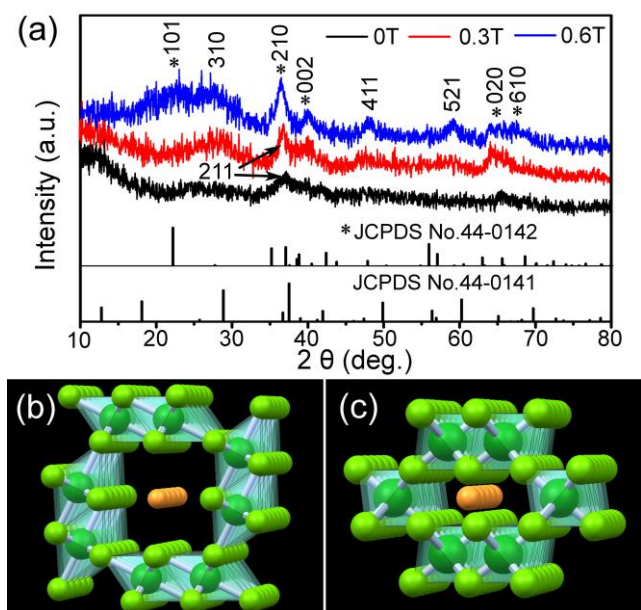


**Fig. 3** (a) XRD patterns of the MnO<sub>2</sub> synthesized at different magnetic fields. The transition of MnO<sub>2</sub> crystal structure induced from (b)  $2 \times 2$  to (c)  $1 \times 2$  tunnels.

5 The corresponding TEM images are shown in Fig. 4. Under normal conditions, these nanoflowers are composed of untrathin nanosheets homogeneously (Fig. 4a). When 0.3T magnetic field was applied, there were many MnO<sub>2</sub> nanoneedles (Fig. 4c) formed which evolved from the initial nanosheets. The lattice

10 fringes in Fig. 4d are explicitly clear with a  $d$ -spacing of 0.3 nm for the (310) plane of the tetragonal phase  $\alpha$ -MnO<sub>2</sub>; the FFT pattern suggests the single crystal character. Strikingly, when at up to 0.6T, the size of the nanoneedles increases and some nanowires form (Fig. 4e). The lattice fringes demonstrate the

15 orthorhombic phase  $\gamma$ -MnO<sub>2</sub> due to the  $d$ -spring corresponding its plane (Fig. 4f). Moreover, both HRTEM image and FFT pattern (inset of Fig. 4f) indicate preferential growth along the (001) direction (c axis), which further confirmed its tunnel direction (Fig. 3c). As a result, it could be speculated that MnO<sub>2</sub> crystallites

20 may easily grow along the magnetic lines of force to form nanowires rather than randomly particles or aggregate spheres, which is similar to the growth of single-crystalline Fe<sub>3</sub>O<sub>4</sub> nanowires<sup>[13]</sup>. Furthermore, the fast diffusion of paramagnetic ions including K, Mn and O would increase the chemical reaction,

25 leading to the decrease of oxygen vacancies and better crystallinity, hence making the formation of nanowires easier and longer<sup>[21-22]</sup>.

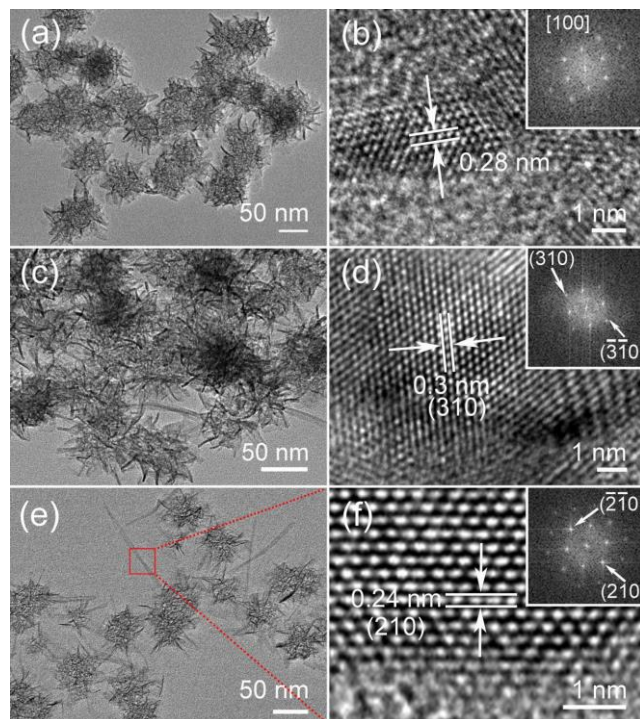


**Fig. 4** TEM images of (a) MnO<sub>2</sub> nanoflowers at 0T, (c) nanoflower-needles at 0.3T and (e) nanoflower-wires at 0.6T. HRTEM images of (b) the MnO<sub>2</sub> nanoflower, (d) nanoflower-needles and (f) nanoflower-wires. Insets are the corresponding FFT diffraction patterns.

Fig. 5 is the hysteresis loops of the samples, the characteristic behaviors of the superparamagnetic particles are detected and the magnetization loops do not show hysteresis or saturate even at 18 KG. It seems that all MnO<sub>2</sub> nanostructures exhibit superparamagnetic behavior, which was caused by the total magnetization decrease owing to the increased dispersion in the exchange integral<sup>[23]</sup>. Especially, all the magnetic susceptibilities

40 of these MnO<sub>2</sub> nanostructures are low and gradually decrease along with the magnetic field increasing. It should be attributed to the high shape anisotropy and the pinning of the magnetic domains in the MnO<sub>2</sub> nanoneedles and nanowires, which might be responsible for the lower magnetic susceptibility than that of the nanoflowers<sup>[13]</sup>. In addition, a trace of K element (Fig. S1†) introduced into the interlayer of the ramsdellite during the growth determines the local ratio of Mn<sup>3+</sup>/Mn<sup>4+</sup>, which could be the reason for the lowest magnetic susceptibility of the nanoflower-wires<sup>[24]</sup>. Therefore, the results imply that there was a close

50 relationship between the magnetic strength with the morphology, crystal structure and magnetic properties of the MnO<sub>2</sub>, which, in tune, could have a direct effect on the electrochemical properties of the materials, as detailed later.

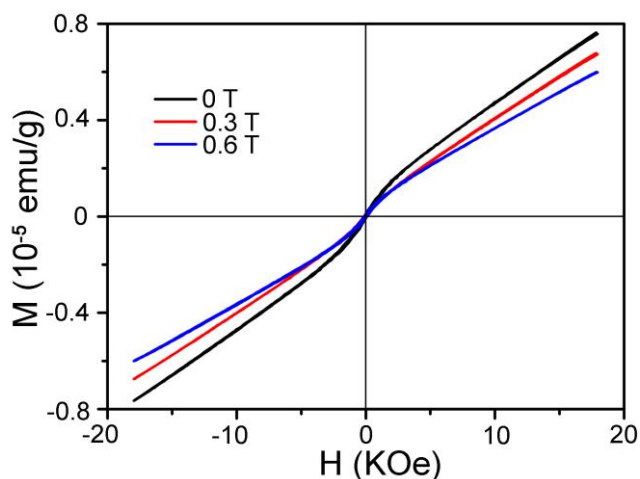


**Fig. 5** Magnetic hysteresis curves measured for the MnO<sub>2</sub> prepared at 0, 0.3 and 0.6T, respectively.

The electrochemical performance of MnO<sub>2</sub> electrodes prepared with an external magnetic field is investigated here. We have studied the advantages of as-fabricated MnO<sub>2</sub> electrodes by cyclic voltammetry (CV) and galvanostatic charge-discharge (CD) measurements in 0.5 M Na<sub>2</sub>SO<sub>4</sub> solution. Fig. 6a shows the CV curves of the MnO<sub>2</sub> electrodes prepared with 0, 0.3 and 0.6 T, respectively, at 50 mV/s. Apparently, the curves of the electrodes with 0.3 and 0.6 T are almost optimal rectangular, which is much better than that of the electrode with 0 T, indicating an excellent capacitance behavior and fast charging-discharging process characteristic. Besides, the integrated area of 0.3T electrode is larger than 0.6T electrode, exhibiting the larger specific capacitance ( $C_{sp}$ ) (216 F/g with 0.3T, 192 F/g with 0.6T), and they are all much larger than 0T electrode (121 F/g). The  $C_{sp}$  versus scan rates are summarized in Fig. 6b (their corresponding curve showing in Fig. S2a, c, e†), demonstrating that  $C_{sp}$  of 0.3T electrode is 1~2 times higher in all scan rates compared with 0T electrode, and also better than that of 0.6T electrode. Especially, when the scan rate is 1 mV/s, the  $C_{sp}$  of 0.3T electrode is up to 382 F/g. Fig. 6c is the CD curves of three electrodes at 0.5 A/g. A high symmetric nature is observed in all charge-discharge curves, indicating a good electrochemical capacitive characteristic and superior reversible redox reaction. The  $C_{sp}$  value calculated from the discharge curves for 0.3 and 0.6T electrode is 306 and 240 F/g respectively, while the  $C_{sp}$  value of 0T electrode is only 196 F/g. The summary plots of  $C_{sp}$  versus current densities (Fig. 6d, their corresponding curve showing in Fig. S2b, d, f†) demonstrate that 0.3T electrode exhibits significantly enhanced capacitance performance. Besides these two types of nanostructures, the 0.3T electrode also exhibit an enhanced specific capacitance compared with the values of other MnO<sub>2</sub> electrode materials reported in the literature, such as ultrafine MnO<sub>2</sub> nanowires (279 F/g), highly ordered MnO<sub>2</sub> nanowire array (254 F/g) and  $\alpha$ -MnO<sub>2</sub> hollow spheres (167 F/g),<sup>[25-27]</sup> further confirming an advantages of the MnO<sub>2</sub> electrode prepared with an external magnetic field.

Fig. 6e shows the Nyquist plots of 0, 0.3 and 0.6T electrodes. For 0.3T electrode, a lower equivalent series resistance (ESR) value (0.21  $\Omega$ ) than 0T (1 $\Omega$ ) and 0.6T electrode (0.67 $\Omega$ ) was obtained, especially a more vertical line in the low-frequency region can be seen, indicating that the 0.3T MnO<sub>2</sub> electrode

provides an ideal pathway for ion and electron transport without kinetic limitations and has a higher conductivity, confirming the magnetic field could improve the electric conductivity of the MnO<sub>2</sub> electrode. The cycle life is another important factor for supercapacitors, hence the long-term cycle stability of 0 and 0.3T electrodes is evaluated at 50 mV/s for 5000 cycles, Fig. 6f. It can be found that the specific capacitance increases gradually and then decreases slightly, indicating an initial activation process for the MnO<sub>2</sub> electrodes. After 5000 cycles, the  $C_{sp}$  based on 0 and 0.3T electrodes retain 80% and 95.3% of their initial capacitance respectively, demonstrating 0.3T electrode is highly stable during such a long term cycling test.

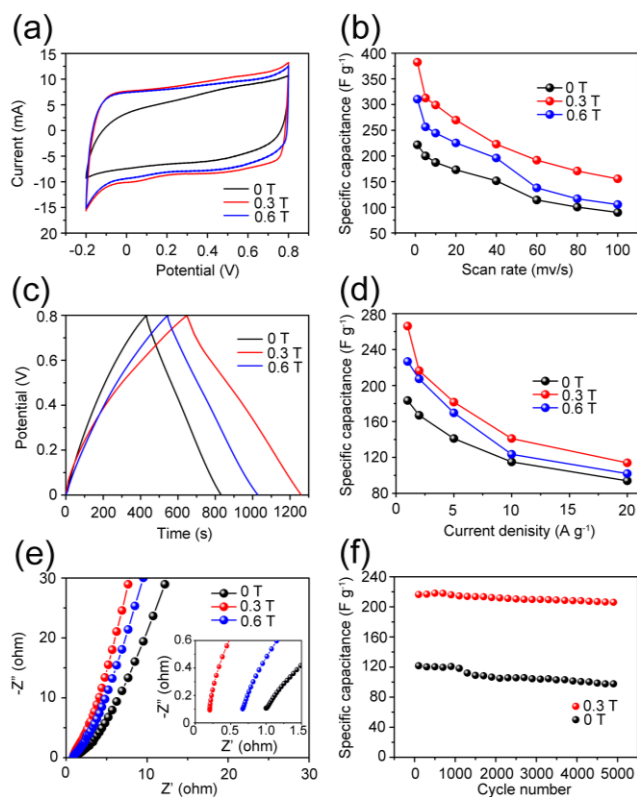


**Fig. 6** (a) CV curves scanning at 50 mV/s, (b) Specific capacitances at various scan rates, (c) charge-discharge curves at 0.5 A/g, (d) Specific capacitances at different current densities, (e) Nyquist plots of 0, 0.3 and 0.6T MnO<sub>2</sub> electrodes, inset shows the high-frequency region of Nyquist plots, (f) cycling stability of 0 and 0.3T MnO<sub>2</sub> electrodes at 50 mV/s.

Based on the above discussion, these results confirm that the MnO<sub>2</sub> nanoflower-needles prepared under 0.3T external magnetic field allow a maximum electrochemical performance, and this could be attributed to the following merits: (i) nanoflower-needles with small diameters offer more accessible electroactive sites for charge transfer and the access of electrolyte ions, (ii) the relatively large  $2 \times 2$  tunnels of  $\alpha$ -MnO<sub>2</sub> formed by octahedral units significantly increase the electrolyte-material contact area and enhance ion diffusion, thus improving the utilization rate of the electrode materials,<sup>[28]</sup> (iii) the lower ESR value, especially, the utilization rate of the electrode material also can be largely enhanced by the high conductivity because of the slight polarization.<sup>[29]</sup> For 0.6T electrode, although new orthorhombic phase appeared, loss of surface area and less active sites occurs because of the small tunnel structure of  $\gamma$ -MnO<sub>2</sub> ( $1 \times 2$  tunnels),

thus the diffusion of Na<sup>+</sup> ions is limited and some voids or pores become inaccessible. Especially, due to the K<sup>+</sup> insertion during the forming of the nanoflower-wires, MnO<sub>x</sub> involving trivalent Mn(III) shows lower conductivity when compared with MnO<sub>2</sub> owing to the Jahn-Teller distortion of the Mn(III)O<sub>6</sub> octahedron.<sup>[2]</sup> That could be the reason why 0.6T electrode exhibits lower C<sub>sp</sub> values than those of 0.3T electrode.

#### 4. Conclusions

In conclusion, an effective magnetic-field-assisted hydrothermal synthesis was used to induce the growth of MnO<sub>2</sub> nanostructures for the supercapacitor application. With the magnetic field assisted, the morphology and crystal structure can be prepared controllably. The MnO<sub>2</sub> nanostructures synthesized under the magnetic strength of 0.3T displayed enhanced C<sub>sp</sub> of 306 F/g at 0.5 A/g and desirable cyclic stability, making them a promising electrode material for supercapacitors. Such intriguing method may open up the possibility of constructing high-performance supercapacitor materials.

#### Acknowledgements

This work was financially supported by the National Natural Science Foundation of China (Grant Nos. 21171035 and 51302035), the Key Grant Project of Chinese Ministry of Education (Grant No. 313015), the PhD Programs Foundation of the Ministry of Education of China (Grant Nos. 20110075110008 and 20130075120001), the National 863 Program of China (Grant No. 2013AA031903), the Science and Technology Commission of Shanghai Municipality (Grant No. 13ZR1451200), the Fundamental Research Funds for the Central Universities, the Shanghai Leading Academic Discipline Project (Grant No. B603), and the Program of Introducing Talents of Discipline to Universities (No. 111-2-04).

#### Notes and references

<sup>a</sup> School of material engineering, Shanghai university of engineering science, Shanghai 201620, China. E-mail: xiyingzhou@yahoo.com

<sup>b</sup> State Key Laboratory for Modification of Chemical Fibers and Polymer Materials, College of Materials Science and Engineering, Donghua University, Shanghai 201620, China. E-mail: hu.junqing@dhu.edu.cn

† Electronic Supplementary Information (ESI) available: [Experimental process, Supplementary Fig.s]. See DOI: 10.1039/b000000x/

‡ These authors contributed equally to this work.

- 1 P. Simon, Y. Gogotsi, Nat. Mater., 2008, 7, 845-854.
- 2 G. Wang, L. Zhang, J. Zhang, Chem. Soc. Rev., 2012, 41, 797-828.
- 3 L. Yang, S. Cheng, Y. Ding, X. Zhu, Z. L. Wang and M. Liu, Nano Lett., 2012, 12, 321-325.
- 4 Z. Chen, V. Augustyn, J. Wen, Y. Zhang, M. Shen, B. Dunn and Y. Lu, Adv. Mater., 2011, 23, 791-795.
- 5 T. Brezesinski, J. Wang, S. H. Tolbert and B. Dunn, Nat. Mater., 2010, 9, 146-151.

- 6 L. F. Chen, Z. H. Huang, H. W. Liang, Q. F. Guan and S. H. Yu, Adv. Mater., 2013, 25, 4746-4752.
- 7 W. Wei, X. Cui, W. Chen and D. G. Ivey, Chem. Soc. Rev., 2011, 40, 1697-1721.
- 8 Z.P. Feng, G.R. Li, J.H. Zhong, Z.L. Wang, Y.N. Ou and Y.X. Tong, Electrochem. Commun., 2009, 11, 706-710.
- 9 J. Duay, S. A. Sherrill, Z. Gui, E. Gillette and S. B. Lee, Acs Nano, 2013, 7, 1200-1214.
- 10 S. Roshny, R. Ranjusha, M. S. Deepak, N. Sanoj Rejinold, R. Jayakumar, S. V. Nair and A. Balakrishnan, RSC Advances, 2014, 4, 15863-15869.
- 11 J. Hone, M. C. Llaguno, N. M. Nemes, A. T. Johnson, J. E. Fischer, D. A. Walters, M. J. Casavant, J. Schmidt and R. E. Smalley, Appl. Phys. Lett., 2000, 77, 666-668.
- 12 X. L. Xu, G. Friedman, K. D. Humfeld, S. A. Majetich and S. A. Asher, Chem. Mater., 2002, 14, 1249-1256.
- 13 J. Wang, Q. W. Chen, C. Zeng and B. Y. Hou, Adv. Mater., 2004, 16, 137-140.
- 14 M. J. Hu, Y. Lu, S. Z., S. R. Guo, B. Lin, M. Zhang and S. H. Yu, J. Am. Chem. Soc., 2008, 130, 11606-11607.
- 15 Y. Lu, L. Dong, L. C. Zhang, Y. D. Su, S. H. Yu, Nano Today, 2012, 7, 297-315.
- 16 L. Dong, Y. Liu, Y. Lu, L. Zhang, N. Man, L. Cao, K. Ma, D. An, J. Lin, Y. J. Xu, W. P. Xu, W. B. Wu, S. H. Yu, and L. P. Wen, Adv. Funct. Mater., 2013, 23, 5930-5940.
- 17 M. R. Gao, S. R. Zhang, Y. F. Xu, Y. R. Zheng, J. Jiang and S. H. Yu, Adv. Funct. Mater., 2014, 24, 916-924.
- 18 V. Subramanian, H. W. Zhou and B. Q. Wei, J. Power Sources, 2006, 159, 361-364.
- 19 J. Luo, H. T. Zhu, H. M. Fan, J. K. Liang, H. L. Shi, G. H. Rao, J. B. Li, Z. M. Du and Z. X. Shen, J. Phys. Chem. C, 2008, 112, 12594-12598.
- 20 W.Y. Li, Q. Liu, Y.G. Sun, J.G. Sun, R.J. Zou, G. Li, X. H. Hu, G. S. Song, G.X. Ma, J.M. Yang, Z. Z. Chen and J.Q. Hu, J. Mater. Chem., 2012, 22, 14864-14867.
- 21 M. Fujiwara, K. Chie, J. Sawai, D. Shimizu and Y. Tanimoto, J. Phys. Chem. B, 2004, 108, 3531-3534.
- 22 M. Z. Wu, Y. Xiong, Y. S. Jia, H. L. Niu, H. P. Qi, J. Ye and Q. W. Chen, Chem. Phys. Lett., 2005, 401, 374-379.
- 23 S.R. Elliott, Physics of Amorphous Materials, Longman, London, New York, 1984, p. 350.
- 24 P. Umek, A. Gloter, M. Pregelj, R. Dominko, M. Jagodic, Z. Jaglicic, A. Zimina, M. Brzhezinskaya, A. Potocnik, C. Filipic, A. Levstik and D. Arcon, J. Phys. Chem. C, 2009, 113, 14798-14803.
- 25 H. Jiang, T. Zhao, J. Ma, C. Yan and C. Li, Chemical communications, 2011, 47, 1264-1266.
- 26 C. L. Xu, S. J. Bao, L. B. Kong, H. Li and H. L. Li, Journal of Solid State Chemistry, 2006, 179, 1351-1355.
- 27 M. Xu, L. Kong, W. Zhou and H. Li, Journal of Physical Chemistry C, 2007, 111, 19141-19147.
- 28 S. W. Donne, A. F. Hollenkamp and B. C. Jones, J. Power Sources, 2010, 195, 367-373.
- 29 Q. Li, Z. L. Wang, G. R. Li, R. Guo, L. X. Ding and Y. X. Tong, Nano Lett., 2012, 12, 3803-3807.